Triblock Protein Copolymers Forming Supramolecular Nanotapes and pH-Responsive Gels

Aernout A. Martens,[†,‡,§] Giuseppe Portale,[||] Marc W. T. Werten,[†] Renko J. de Vries,[‡] Gerrit Eggink,[†] Martien A. Cohen Stuart,[‡] and Frits A. de Wolf*[,†,§]

Biobased Products, Agrotechnology & Food Sciences Group, Wageningen UR, Bornsesteeg 59, 6708 PD Wageningen, The Netherlands, Laboratory of Physical Chemistry and Colloid Science, Agrotechnology & Food Sciences Group, Wageningen UR, Dreijenplein 6, 6703 HB Wageningen, The Netherlands, Dutch Polymer Institute (DPI), John F. Kennedylaan 2; 5612 AB, Eindhoven, The Netherlands, and European Synchrotron Radiation Facility, 6 Rue Jules Horowitz, BP 220, 38043 Grenoble, Cedex 9, France

Received August 28, 2008; Revised Manuscript Received December 10, 2008

ABSTRACT: We report on the biosynthesis of 65 kDa A−B−A triblock copolymers consisting of pH-responsive (acidic) silklike blocks and nonresponsive collagenlike blocks, and we show that at pH values where the silklike blocks become uncharged, these polymers form transparent high-modulus gels, that is, 7−15 kPa at 8 g·L^{-1}, that consist of supramolecular nanotapes with a height of 2.8 nm, a width of ∼14 nm, and an average length of >10 μm. At the concentrations employed, both of these protein triblocks essentially form the same structure, irrespective of block order. The amount of product isolated from the extracellular medium is in the gram per liter range. This high yield makes various applications of this promising class of biocompatible materials possible.

Introduction

Stimulus-responsive, nanostructured, and self-assembling polymer materials are essential for high-value applications such as self-healing coatings, chemomechanical fibers, sensors, smart packaging, surgery, regenerative medicine, and pharmaceutics.[1−7] Speed and precision of stimulus-induced supramolecular self assembly are expected to benefit from the use of polymers built from chiral monomers and consisting of one single molecular type with exactly defined length, domain structure, and monomer sequence. Whereas chemically synthesized polymers normally lack these features, they are the hallmark of biosynthetic proteins. In addition, chemical polymers typically lack proteinborne biocompatible features such as cell attachment sites or programmed biodegradation, which are exploitable in regenerative medicine and pharmaceutics. These considerations are the basis of the rapidly expanding field of protein polymer science, which focuses on nature-inspired designer proteins with a structure-forming function.[8]

The stimulus-responsive formation of nanostructures is a feature that is typically obtained with block copolymers. In chemical triblock copolymers, the order of the blocks normally determines the supramolecular organization in solution. A polymer with soluble end blocks and an insoluble middle block usually assembles into micelles, vesicles, or lamellar structures.[9] A polymer with insoluble end blocks and a soluble middle block can form, in addition, molecular networks and gels, provided the concentration is high enough.[10]

In the present work, we investigate the self-assembly behavior of novel, entirely biosynthetic triblock copolymers built from two selected monodisperse block types. One block (**S**) is a 192-amino-acid-long pH-responsive silklike octapeptide repeat,[11] $[(Gly\text{-}Ala)_3\text{-}Gly\text{-}Glu]_{24}$, that is capable of forming crystalline stacks of antiparallel Ala-Gly-Ala-Gly-Ala β sheets[11] bordered by Gly-Glu-Gly γ turns.[11,12] At neutral to alkaline pH, that is, in the polyanionic state, its glycine-rich chain assumes a random extended conformation[13] and is well soluble in water. Conversely, at low pH, that is, in its uncharged state, it is insoluble.[13] The other block (**C**) is a 198-amino-acid-long extremely hydrophilic glutamine-, asparagine-, and serine-rich collagenlike designer polypeptide that our group developed.[14] It has a strong preference for unordered structure at all pH values and does not form supramolecular collagenlike assemblies because of an absence of prolyl hydroxylation.[14] It has the ability to direct human cells in culture selectively to patches of a substrate that are coated with the polypeptide[15] and has favorable biocompatibility as compared with animal collagen-derived products in blood applications.[16] Two complementary arrangements of these blocks are compared, namely, two consecutive silklike blocks in the middle flanked by two collagenlike blocks at the N- and C-terminal ends of the molecule (**CSSC**) and vice versa (**SCCS**). Both triblock copolymers were produced in high yield in the methylotrophic yeast *Pichia pastoris* and were purified using an easy and scalable procedure. Surprisingly, both polymers formed similar hydrogels consisting of tapes with extremely high aspect ratio in dilute aqueous solution at low pH. These new polymers are a valuable basis for the development of various biomaterials.

Results

Production of Two Large Block Copolymers with Complementary Block Order. The two 802-amino-acid-long block copolymers that comprise the above-mentioned monodisperse silklike, **S**, and collagenlike, **C**, blocks in the order **CSSC** and **SCCS** were readily produced and secreted by *P. pastoris* (Figure 1). After a few simple differential precipitation steps that were chosen to be compatible with eventual scale up (Experimental Section), 1.1 g of dry **CSSC** and 1.9 g of dry **SCCS** were recovered per liter of cell-free medium. The remaining contamination with exopolysaccharides was 0.04 g per gram of dry product, whereas, on the basis of the amino acid composition of the product and the analysis procedure described in the Experimental Section, the **CSSC** content was estimated to be 0.99 mol per mole of protein, and the **SCCS**

* To whom correspondence should be addressed. E-mail: frits.dewolf@wur.nl.
[†] Biobased Products, Wageningen UR.
[‡] Laboratory of Physical Chemistry and Colloid Science, Wageningen UR.
[§] Dutch Polymer Institute.
[||] European Synchrotron Radiation Facility.

10.1021/ma801955q CCC: $40.75
Published on Web 01/21/2009

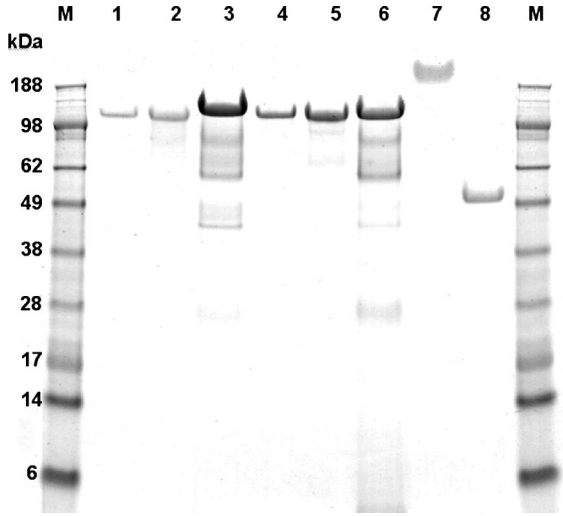

Figure 1. SDS-PAGE of **CSSC** and **SCCS** as originally present in the cell-free fermentation broth and after recovery by selective precipitation, freeze drying, and resolubilization. Lanes M: molecular mass markers; lanes 1,2: different amounts of recovered **CSSC**; lane 3: cell-free broth with **CSSC**; lanes 4,5: different amounts of recovered **SCCS**; lane 6: cell-free broth with **CSSC**; lane 7: isolated **CC**; lane 8: isolated **SS**.

content was estimated to be 0.98 mol per mole of protein. According to mass spectrometry (MALDI-TOF) and sequencing of the first six N-terminal amino acids of the precipitated product, the molecular mass and N-terminal sequence of the **CSSC** and **SCCS** corresponded to those of the products as designed after correct precursor processing by *P. pastoris*. In SDS-PAGE, **CSSC** (Figure 1, lanes 1−3) and **SCCS** (Figure 1, lanes 4−6) appeared to migrate slowly relative to the proteins used as molecular mass markers (Figure 1, lane M), resulting in an apparent molecular mass of ∼135 kDa, that is, about twice the real mass. This effect is typical of such highly polar and acidic polymers with a large content of small amino acids and has been previously documented.[11,13,14] For comparison, the highly hydrophilic **CC** block[14] without the **S** blocks attached to it migrates even slower (Figure 1, lane 7), whereas the isolated (free) **SS**[13] migrates faster than the full-length **CSSC** and **SCCS** (Figure 1, lane 8) but slower than expected according to the molecular mass of **SS** (28 kDa).[13] Thus, the electrophoretic behavior of both **CSSC** and **SCCS** is intermediate between that of **CC** and **SS**. On the basis of densitometric analysis of the product bands after SDS-PAGE, the concentration of **CSSC** and **SCCS** in the cell-free fermentation broths was estimated to be 4.5 to 6.5 g product per liter, which is in general accordance with the previously reported production and secretion of isolated (free) **CC**,[14] **SS**,[13] and other heterologous proteins.[17,18]

Gel Formation upon Charge Neutralization. Both **CSSC** and **SCCS** were water soluble at pH 7. After acidification to pH 2 to 4, 20 g·L^{-1} solutions of both polymers formed a transparent gel, which dissolved again when the pH was shifted to alkaline values. For comparison, the free **SS** was previously shown to be soluble at neutral to alkaline pH and to form sedimenting flocks rather than gels at low pH,[13] whereas the previously produced free **CC**[14] appeared in the present study to be soluble over a wide pH range, down to at least pH 2. The formation of gels is probably triggered by mutual interactions between the **S** blocks.

The behavior of the **CSSC** and **SCCS** gels during dynamic (oscillating) deformation was investigated by means of rheometry (Figure 2). At strain values up to about 1%, the storage modulus of 8 g·L^{-1} of **CSSC** and **SCCS** gels was a factor of 325 and 180 times larger, respectively, than the loss modulus. Between 1 and 6% strain, both polymer gels revealed strain

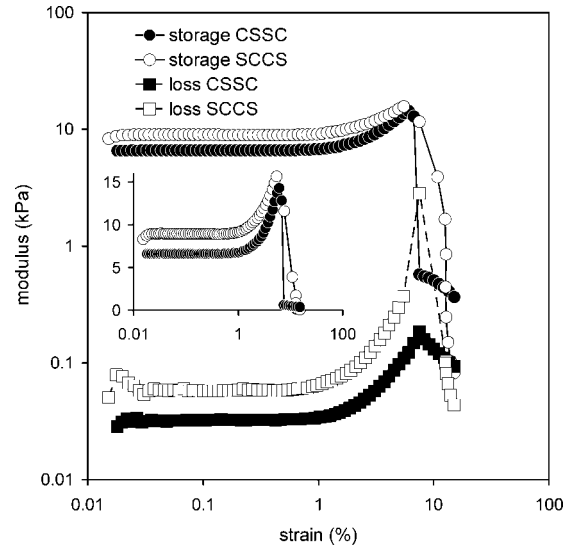

Figure 2. Rheometric analysis of the effect of dynamic deformation (strain) on **CSSC** and **SCCS** gels. The moduli of **CSSC** and **SCCS** are shown by closed and open symbols, respectively: ●,○: storage moduli (G'); ■,□: loss moduli (G''). The inset shows the storage moduli on a linear scale, to outline the strain hardening. The pH was approximately 1.5, the polymer concentration 8 g·L^{-1}, the oscillation frequency 1 Hz and the sampling time 1 min per strain value.

hardening (Figure 2, inset with linear scaling). At larger strain, the storage moduli steeply dropped and never returned to the original value when smaller strains were subsequently tested, indicating that the gels were broken. The similar storage moduli, strain hardening profiles, and breakage points of **CSSC** and **SCCS** gels indicate structural similarity of the two gels.

Supramolecular Tapes. Similar behavior of **CSSC** and **SCCS** at low pH is also illustrated by the supramolecular structure emerging from transmission electron microscopy (TEM) of uranyl-acetate-stained and successively dried preparations (Figure 3a,b), which showed **CSSC** and **SCCS** fibrils. The dried fibrils of **SCCS** frequently form bundles, whereas bundles were seldom seen in dried **CSSC**. The bundles randomly split and converge (Figure 3b).

The presence of supramolecular fibrils was confirmed by tapping mode atomic force microscopy (AFM). Very long supramolecular fibrils were adsorbed to a silica AFM support (Figure 3c,d) that was dipped in acidic **CSSC** or **SCCS** dispersions (0.1 g·L^{-1}, pH 2). From cross-sectional analysis (Figures S1−S4 in the Supporting Information), similar fibril heights for **CSSC** and **SCCS** of 1.7 to 2.2 nm and 1.1 to 2.0 nm, respectively, and the same apparent width of 20−23 nm were deduced. The typical radius of curvature of the tip of the AFM probe was 2 nm, with a guaranteed maximum of 5 nm. Therefore, the real width of the dry fibrils in the AFM micrographs was at least 10 nm and at most 23 nm. From AFM and TEM images we estimate that at least 90% of the fibrils are longer than 10 μm. According to these measurements, the dry **CSSC** and **SCCS** fibrils are tapes that resemble those reported for three related dry systems as follows: (1) dry fibrils of the isolated **SS** block deposited at low concentration from methanol,[13] (2) polyethylene-oxide-conjugated $[(Gly\text{-}Ala)_3\text{-}Gly\text{-}Glu]_{20}$ deposited from a methanol formic acid mixture,[19] and (3) nonconjugated $poly[(Gly\text{-}Ala)_3\text{-}Gly\text{-}Xaa]_{84}$ with Tyr, Glu, His, and Lys residues in consecutive Xaa positions deposited from water.[20]

Fibrils were not observed in TEM and AFM samples prepared within half an hour of acidification of the **SCCS** or **CSSC** solution. Samples taken from 2 h onward contained many fibrils, indicating that these fibrils form in the course of hours. This

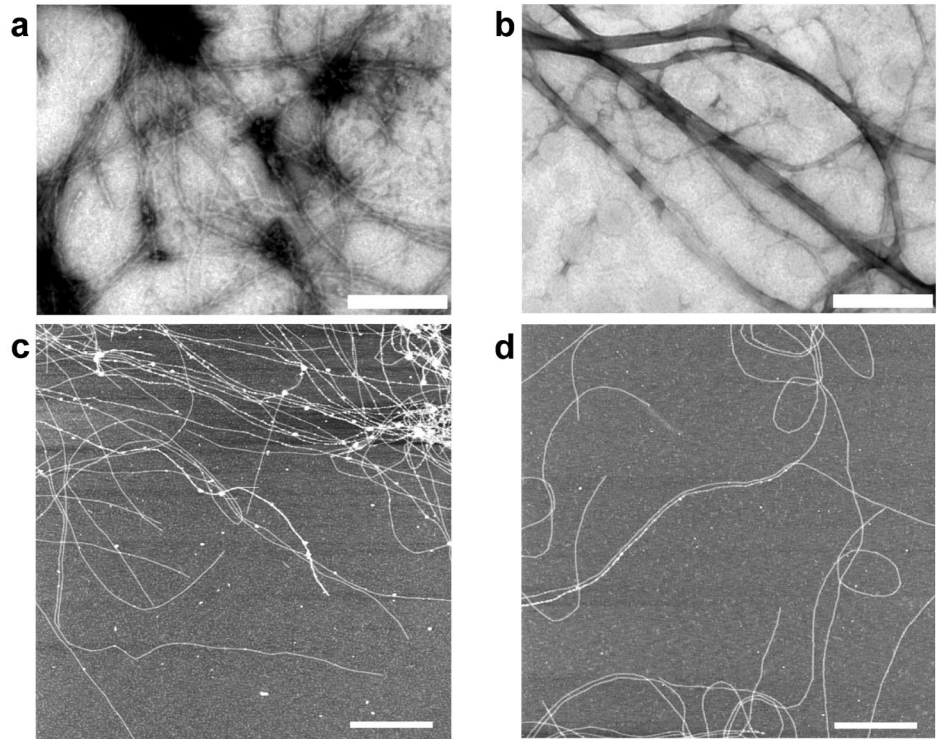

Figure 3. Micrographs of supramolecular **CSSC** and **SCCS** fibrils formed at pH 2. (a,b) TEM images of **CSSC** and **SCCS** fibrils, respectively, deposited on Formvar. The white bars correspond to 200 nm. (c,d) Atomic force micrographs of **CSSC** and **SCCS** fibrils, respectively, deposited on silica. Higher objects are lighter in color. The white bars correspond to 1 μm. The fibrils in all four micrographs were deposited from a 0.1 $g \cdot L^{-1}$ protein solution.

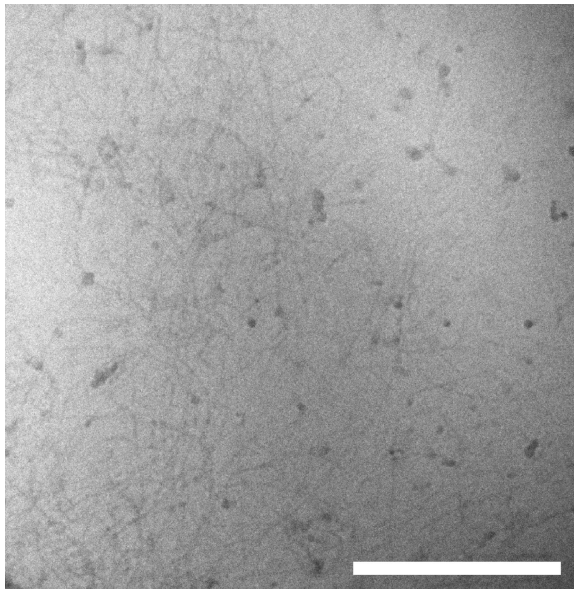

Figure 4. Cryo-TEM micrograph of supramolecular **CSSC** fibrils formed at pH 2. The white bar corresponds to 500 nm. The preparation was not stained. The irregularly shaped clumplike 20−50 nm structures are ice crystals. The brightness and contrast settings of the entire image were adjusted to 50 and 30%, respectively, in Paintshop Pro 9.01. The original, unprocessed image is available as Figure S5 in the Supporting Information.

observation and also the observation by cryogenic (cryo)-TEM of fibrils in solutions frozen after overnight incubation at pH 2 (Figure 4 and Figure S5 in the Supporting Information) reveal that the formation of fibrils was not merely due to the process of drying the acidified dispersions for subsequent microscopic analysis. Whereas the low contrast of the cryo-TEM images such as in Figure 4 did not allow us to determine the dimensions of the hydrated fibrils in **CSSC** and **SCCS** gels, those dimensions can be deduced from small-angle X-ray scattering (SAXS) profiles recorded from 20 $g \cdot L^{-1}$ gels (Figure S6 in the Supporting Information). The SAXS patterns were best interpreted in terms of a rectangular fibril cross section (tape structure) with a height of 2.8 nm for both **CSSC** and **SCCS**, a width of 13.6 nm for **CSSC**, and a width of 14.3 nm for **SCCS**. Both widths of hydrated fibrils are within the range that was observed for the dry fibrils with AFM. The SAXS deduced height is somewhat larger than the 1.1 to 2.2 nm height observed for dry fibrils with AFM. Because SAXS is noninvasive and was performed on fibrils in aqueous environment, the X-ray data probably more closely reflect the size of the hydrated fibrils than the AFM measurements of dry fibrils do.

Effect of pH on Secondary Structure. Changes in secondary structure induced by shifting the pH from 7 to 2 were followed using circular dichroism (CD) and were compared with the effect of a similar pH shift on the isolated **CC** or **SS**.[13] At pH 7 (or above), the CD spectra of **CSSC** (Figure 5a) and **SCCS** (Figure 5b) revealed a combination of random and extended structure, just like the isolated **SS**.[13] Whereas the isolated (free) **SS** became turbid because of random aggregation at low pH,[13] both **CSSC** and **SCCS** formed a transparent gel that allowed the recording of UV−CD spectra down to at least pH 2 (Figure 5a,b). The secondary structure of specifically the **S** block in **CSSC** and **SCCS** can probably be followed at low pH by subtracting the **CC** spectrum from the **CSSC** and **SCCS** spectra because the isolated **CC** maintains unordered structure at low as well as neutral to alkaline pH (Figure 5c) and because at least at pH 7, the sum of the **CC** and **SS** spectra closely matched that of the **CSSC** or **SCCS** spectra (Figure 5d). The result of such an **S**-block-revealing subtraction at low pH is shown in Figure 5e. The combination of a negative band around 208 nm and positive bands around 200 and 225 nm, seen in both the original and subtracted spectra, indicates that the **S** block is rich in β turns[13,21]

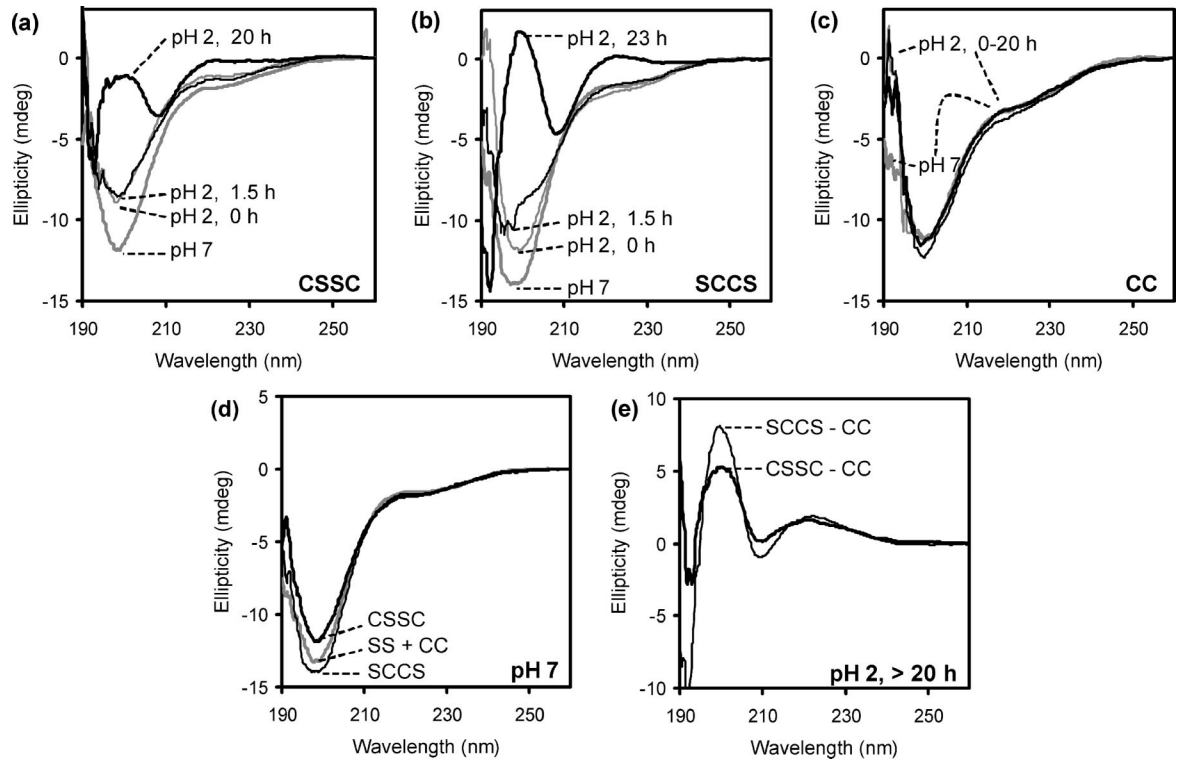

Figure 5. CD spectra of **CSSC** and **SCCS** and their constituent blocks, at pH 7 and 2. (a,b) Spectra of **CSSC** and **SCCS**, respectively, measured at pH 7 immediately after adjustment to pH 2 and 1.5−23 h after adjustment to pH 2, as indicated in the graph. (c) Spectra of isolated **CC**, without any **S** blocks attached, at pH 7 and 2. (d) Spectra of **CSSC** and **SCCS** compared with the sum of the spectra separately obtained from isolated **SS** without any **CC** block attached and from isolated **CC**, all at pH 7. Before summation, the **CC** and **SS** spectra were normalized to reflect amounts of **CC** and **SS** that were equimolar to **CSSC** and **SCCS**. (e) Calculated spectra of the **S** blocks in **CSSC** and **SCCS** obtained by subtraction of the **CC** spectrum from the **CSSC** and **SCCS** spectra, all measured after incubation for at least 20 h at pH 2. Before subtraction, the **CC** spectrum was normalized to reflect an amount of **CC** equimolar to **CSSC** and **SCCS**. Polymer concentration was 0.09 $g \cdot L^{-1}$ at pH 2 and 0.1 $g \cdot L^{-1}$ at pH 7 in a 1 mm cuvette thermostatted to 20 °C.

at low pH. The deduced **S** block spectra closely resemble those of isolated **SS** dried from an aqueous medium onto a quartz substrate[13] and of poly[(Gly-Ala)$_3$-Gly-Xaa] with Tyr, Glu, His, and Lys residues in consecutive X positions.[22] In agreement with the above-mentioned observation that fibrils were not seen immediately after acidification, the development of the secondary structure shown in Figure 5e took several hours.

Discussion

Same Tape Structure Irrespective of Block Order. This work describes for the first time high-molecular-weight silk collagen triblock copolymers with two complementary arrangements of self-assembling and nonassembling inner and outer blocks. Most interestingly, polymers with the self-assembling **S** blocks in the middle or at the ends of the molecule both organized into thin and extremely long tapes and both formed gels. The essential discriminative feature of **CSSC** and **SCCS** with respect to chemical block copolymers is their exactly defined monomer sequence and block length in combination with the chiral nature of all monomer constituents. If the middle blocks in typical chemical polymers are insoluble, then they form nanosized spherical or elongated particles with an amorphous inner phase surrounded by a corona of soluble end blocks that stabilize the particles against aggregation.[9] If the end blocks are insoluble, then similar structures[23] (the middle blocks forming loops) may appear at low concentration, whereas at high concentration, networks and gels can be formed for which end blocks must reside in separate domains.[10] For the biosynthetic **CSSC** and **SCCS**, the driving force for self assembly is not phase separation into an amorphous phase but the folding into a secondary structure accompanied by hydrophobic stacking, which leads to well-defined crystalline tapes with a morphology that is independent of the block order. By chemically attaching polydisperse polyethylene oxide to the N- and C-terminal ends of [(Gly-Ala)$_3$-Gly-Glu]$_{10}$ or [(Gly-Ala)$_3$-Gly-Glu]$_{20}$, the group of van Hest[19] could also prevent isotropic aggregation of the silklike polymer. At high protein concentration and in crystallization-promoting solvent mixtures rather than in water, this resulted in long fibrillar structures similar to ours. The only difference between **CSSC** and **SCCS** seems to be the somewhat increased bundle formation upon drying of **SCCS** tapes observed with TEM (Figure 3b), which may have its origin in the slightly different structures in water for the different block orders. For **CSSC**, the hydrophilic **C** blocks point outward from the **SS** block core, but for **SCCS**, the **CC** blocks form a corona of loops around the core of **S** blocks that are analogous to loops in flowerlike micelles.[23] Also, some of the **SCCS** molecules could bridge two tapes by insertion of their **S** blocks in different tapes rather than in the same tape.

Tape Dimensions. The fibrils are formed at low pH in aqueous solution which, at high concentrations, forms gels. The more a sample of these hydrated fibrils is processed for microscopy by drying or staining, the less representative the image becomes for the fibril in solution. Therefore, the TEM and AFM images must be qualitatively interpreted, although from AFM measurements we can already deduce that **CSSC** and **SCCS** probably form tapes. Also, the group of van Hest found that the fibril height measured with AFM is smaller than the calculated height of a β sheet. This was attributed to deformation of the fibril caused by the AFM tip pressure and the influence of air humidity.[19] Thus, AFM and TEM were used for a qualitative assessment, whereas information about the

dimensions of the **S** block was obtained from X-ray diffraction data from Krejchi et al.[24] The structure of our tapes, which are formed in water, is probably best measured with a noninvasive technique like SAXS, whereas the tapes are kept in water throughout the measurement.

The fibrils most likely consist of a dense core of stacked **S** blocks and a dilute corona of hydrophilic **C** blocks. The corona has, because of the high water content, an electron density that is close to that of water. Therefore, the highest electron density gradient is on the interface of the corona and the core. Because SAXS is sensitive to this density gradient, the main scattering contribution will be that of the core, of which we determined the dimensions according to the Supporting Information.

Structure and Orientation of the Stacked S Blocks. The repetitive $[(\text{Gly-Ala})_3\text{-Gly-Glu}]_n$ structure of the **S** block is that of a protein pioneered by the group of Tirrell.[11] It forms needle-shaped lamellar crystals when subjected to a procedure involving solubilization in 70/30% formic acid/water, replacing these solvents with methanol, and drying. X-ray crystallography indicated that the crystals consist of tightly packed face-to-face, back-to-back stacks of antiparallel β sheets and that each sheet consists of β strands with a length of five amino acids, which are bordered on either end by γ (i.e., three-residue) turns containing glutamic acid.[11,12,24] Furthermore, X-ray crystallography indicated that the orientation of the β sheets was perpendicular to the stacking direction.

However, for three reasons, the core of our **CSSC** and **SCCS** tapes is unlikely to consist of such a stack of β sheets: (1) It is known that upon hydration, the contribution of β sheet in poly[$(\text{Gly-Ala})_3$-Gly-Glu] crystals, dried from methanol, strongly decreases in favor of a contribution of turns and disordered chains. This already occurs at a relative humidity of ~80%, where the water content of the preparations is ~10−15%.[25] (2) The low-pH CD spectra of the **S** blocks in **CSSC** and **SCCS** clearly deviate from the spectra of polypeptides in β-sheet conformation, for example, polylysine,[26] silk II,[27,28] and poly-ethylene-oxide-conjugated poly[$(\text{Gly-Ala})_3$-Gly-Glu] prepared from (methanol-containing) organic solvent.[19] All of these have one dominant negative CD band around 215−220 nm and one dominant positive band around 195 nm. Thus, the present **S**-block spectra indicate a distinct secondary structure of **CSSC** and **SCCS**, which is probably rich in β turns[13,21] and possibly with a contribution from extended structure having another hydrogen bond pattern than antiparallel β sheet. A presence of β turns is not unexpected for a silklike protein because the silk I conformation[29,30] of natural silk is also based on β turns, even though these could be of a different specific type. (3) If the core of the tape would consist of stacked β sheets, then the orientation of the surface of each sheet would probably be perpendicular to the tape's long axis to minimize the contact of the hydrophobic β-sheet surface with the surrounding water and hydrophilic **C** blocks. The stacking direction would thus be parallel to the long axis of the tape and perpendicular to the surface of each sheet, like the stacking direction in crystals formed from dispersions in organic solvent mixtures.[11,13,24] As mentioned in the introduction, **CSSC** contains two adjacent **S** blocks, each consisting of 24 $[(\text{Gly-Ala})_3\text{-Gly-Glu}]$ repeats, that is, 48 repeats in total. A tape consisting of perpendicularly oriented flat **SS** β sheets would then have an expected width of ~23 nm. This is much larger than the values emerging from the present experimental data (tape width of ~14 nm according to SAXS and apparent width of ~17 nm according to AFM).

These three observations suggest that poly[$(\text{Gly-Ala})_3$-Gly-Glu], when stacked in a supramolecular assembly, can adopt two different structures: (1) a flat β sheet when fibrils form in organic solvent and (2) an alternative structure formed in aqueous solutions at low pH, that is, when the glutamic acid residues are uncharged. We are currently investigating the conformation of the **S** block with uncharged glutamic acid residues in water by using MD simulation. This work, which will be published elsewhere, shows that a β-roll conformation in which the alanine side groups point outward at each side of the roll is a more probable conformation in water than a flat, antiparallel β sheet. The simulations suggest that for such β rolls, like for flat antiparallel β sheets, the stacking direction is perpendicular to the surface formed by the side of the β rolls, and the formation of stacks is driven by hydrophobic effects. Again, perpendicular orientation minimizes the contact of the nonpolar flanks of the β rolls with the surrounding water. The length of a chain in β roll conformation is essentially half of the length of such a chain in flat β sheet conformation. In perpendicular orientation, it would be equal to the width of the **SS** stack, and indeed, the length of a β roll of 48 $[(\text{Gly-Ala})_3\text{-Gly-Glu}]$ repeats (~12 nm) approximately matches the width of the tapes measured by SAXS (14 nm).

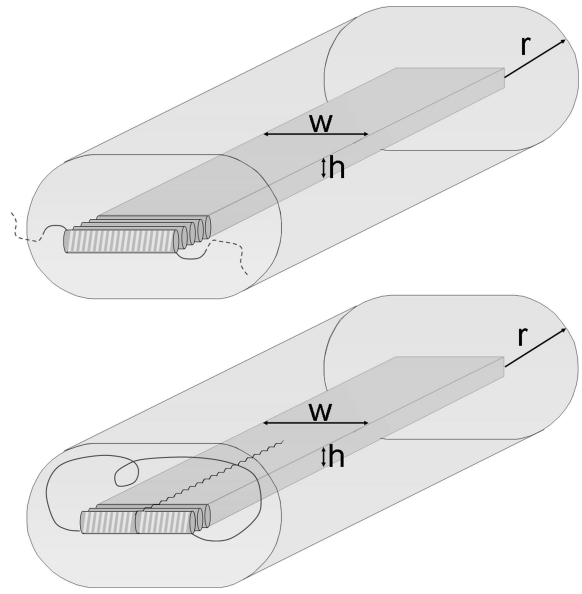

Figure 6. Possible arrangement of **CSSC** (top drawing) and **SCCS** (bottom drawing) in the observed supramolecular tapes formed at pH 2. By stacking on top of each other, the **S** blocks, schematically depicted as white-gray striped bars, form a very long core with a cross section (w, h) of approximately 14 and 2.8 nm, respectively, as measured by SAXS. The **S** blocks in **SCCS** (lower drawing) are proposed to assemble head-to-tail, thus forming a double stack consisting of two parallel stacks of single **S** blocks that together generate the same width (w) as a single stack of **SS** blocks. The extremely hydrophilic **C** blocks are depicted as thin dark wires emerging from the **S** blocks. Because they do not interact with each other and remain in unordered conformation, they are assumed to form a hydrophilic corona with a yet unknown thickness (r) of several nanometers, dictated by the effective density of the **CC** random coil and the repeat distance between consecutive **S** blocks in the core stack.

Structure of the Tapes. Because the **S** blocks appear to be responsible for supramolecular stacking and tape formation and because the hydrophilic **C** blocks do not aggregate and remain in unordered conformation at low pH, the tapes are probably composed of a core of stacked **S** blocks, probably in β-roll conformation, and a corona of unfolded hydrophilic **C** blocks, as schematically depicted in Figure 6.

Even though the length of the terminal **S** blocks in **SCCS** is half of that of the central **SS** blocks in **CSSC**, the width of the **CSSC** and **SCCS** tapes differed by only 5%. Because the secondary structure of the **S** blocks is the same in supramolecular stacks of **CSSC** and **SCCS** and because it is unlikely that their orientation with respect to the tape's long axis would be very

different, this similar width of **CSSC** and **SCCS** tapes probably indicates head-to-tail assembly of **S** blocks in **SCCS**, as schematically indicated in the lower drawing of Figure 6.

Polymer Production. As a precaution, we avoided possible problems associated with premature product self-assembly in the cells or in the fermentation broth by designing the critical value for gel formation to be below the intracellular as well as extracellular pH. Secreted production at pH 5 in *P. pastoris* yielded several grams of polymer per liter of cell-free fermentation broth. This high yield shows that the high molecular weight, the repetitive amino acid sequence, and the amino acid composition with extreme bias toward glycine and, to a lesser extent, alanine, proline and glutamate, did not cause any production problems. Probably because of their highly unusual physical properties, the polymers could be purified from the medium in only a few well-scalable and simple precipitation steps. The process is suitable for the preparation of product quantities that will allow materials testing for medical and other applications.

Outlook. Both the **S** and **C** blocks are likely biocompatible, because silk[31−35] and collagen[36−39] materials are already used for such purposes. The free **C** block was previously shown to have a higher (HeLa) cell-binding capacity than animal B-type gelatin[15] and a favorable biocompatibility in blood applications, as compared with chemically modified animal gelatin.[16] Exposed as loops or fringes in the corona of **SCCS** or **CSSC** tapes, respectively, the **C** block, with its unordered conformation, is ideal for the incorporation of signal-transmitting peptide sequences to direct cell differentiation.[5,40] The formation of very long tapes, which are capable of spanning large distances between contact points in the gel's network, implies that gels can be prepared at low concentrations and thus at relatively low cost because only small quantities of material are needed. For the same reason, the structure of the gel is very open, which allows (human) cells to easily penetrate into the gel.

Conclusions

We have produced biocompatible, entirely biosynthetic protein polymers that are more than 800 amino acids long and are capable of pH-triggered self-assembly into micrometer-long nanotapes and the formation of dilute high-modulus gels. The tapes are probably composed of a core of stacked **S** blocks and a corona of hydrophilic **C** blocks with unordered conformation. We propose that in aqueous environment, the self-assembled **S** blocks adopt a structure other than flat, antiparallel β sheet, possibly a β roll. The polymer production yields were high (grams per liter range), and purification from the fermentation broth was relatively easy, involving only a few precipitation steps. The present class of polymers could be valuable as nanowires in technical applications. In particular, polymers with different amino acids in the Xaa position of the [(Gly-Ala)$_3$-Gly-Xaa] repeats or mixtures of such polymers, in which self-assembly is triggered by mutual interactions closer to physiological pH, could be useful scaffold materials for cell culturing and tissue engineering. For example, one could envisage dual mixtures of negatively and positively charged molecules co-assembling at neutral pH (two-component systems). The two components can be separately produced without a risk of premature self-assembly in the course of the production process

Experimental Section

Generation of Recombinant Strains. A double-stranded adapter for the **C**-block-encoding DNA, created by annealing of the oligonucleotides 5′-AATTCGGTCTCGGTGCTGGTGCACCCG-GTGAGGGTGCCTAAGCGGCCGC-3′ and 5′-GCCAGAGCCAC-GACCACGTGGGCCACTCCCACGGATTCGCCGGCGAGCT-3′, was ligated into an *Eco*RI/*Xho*I-digested pMTL23 vector that had been previously modified to remove its *Bsa*I site.[13] After linearization with *Dra*III and dephosphorylation of the resulting vector, a P2 sequence cut with *Dra*III and *Van*91I from the previously described pMTL23-P2 vector[14] was inserted so as to create the **C**-block-encoding DNA template.

The **S**-block-encoding DNA was created as previously described for the protein EE24[13] (corresponding to **SS**) with the exception that at present, the DNA template consists of 12 rather than the previously used 24 repeats of the [(Gly-Ala)$_3$-Gly-Glu]$_2$-encoding *Bsa*I/*Ban*I fragment.

*Bsa*I and *Ban*I were used to join both templates by directional ligation, first resulting in templates encoding **CS** and **SC** and, subsequently, in templates encoding **CSSC** and **SCCS**. These final templates were cloned into expression vector pPIC9 (Invitrogen) using *Eco*RI and *Not*I. (See below for GenBank accession numbers.) This creates a fusion with the *Saccharomyces cerevisiae* α-mating factor secretion signal present in vector pPIC9 such that correctly processed secreted proteins would have an N-terminal sequence of YVEFGL (six amino acids preceding the N-terminal silk- or collagenlike domain). The resulting vectors were linearized with *Sal*I to promote homologous integration at the *his4* locus upon transformation of *P. pastoris* GS115 by electroporation, as previously described.[17]

Accession Numbers. The DNA sequences (and translated amino acid sequences) of the *Eco*RI/*Not*I fragments encoding **CSSC** and **SCCS** have been deposited in the GenBank database under accession nos. EU202952 and EU202951, respectively. The amino acid sequences of **CSSC** and **SCCS** can also be accessed directly under nos. ABW84222 and ABW84221, respectively.

Polymer Production and Purification. Polymer production was obtained in fed-batch fermentations of *P. pastoris* in 2.5 L Bioflo 3000 bioreactors (New Brunswick Scientific), essentially as previously described.[41] The pH was maintained at 5 throughout the fermentation, and the methanol concentration was maintained at 0.2% (v/v) during the induction phase. The fermentation medium, containing the **CSSC** or **SCCS** product, was separated from the cells by centrifugation (15 min, 20 000 g, 4 °C, Sorvall SLA1500 rotor), followed by microfiltration of the supernatant. Selective precipitation of **CSSC** or **SCCS** from the cell-free medium was induced by the addition of ammonium sulfate to 30% saturation. After 30 min of incubation at 4 °C, the precipitate was recovered by centrifugation (20 min, 8000 g, 4 °C, Sorvall SLA1500 rotor). The polymer pellets were dissolved in 10 mM ammonia (pH 9), the volume of which corresponded to 20% of the cell-free medium, and the precipitation procedure was repeated once. Subsequently, the polymers were selectively precipitated by the addition of acetone to a final concentration of 80% (v/v) and were dissolved again in 10 mM ammonia and precipitated with acetone once more, after which the pellets were resuspended in water and freeze dried for storage. Portions of the salt-containing freeze-dried product (2 to 4 g) were dissolved in 100 mL of 50 mM ammonia and were extensively dialyzed against 10 mM ammonia, after which the desalted product was freeze dried again.

Product Identification and Purity Assessment. The analysis of the amino acid composition after acid hydrolysis was performed using HPLC by Ansynth, Roosendaal, The Netherlands. The content of **CSSC** or **SCCS** was subsequently determined by linear least-squares fitting of (1) the theoretical composition of the pure product and (2) the composition determined for host-derived proteins present in the medium to the data experimentally observed for the dry product recovered from the fermentation broth. The (poly)saccharide content was determined by a phenol−sulfuric acid carbohydrate essay.[42] The molecular mass distribution of the products was analyzed by MALDI-TOF mass spectrometry (Bruker Ultraflex) using sinapinic acid as matrix. The product in various stages of purification was assessed on SDS-PAGE (Invitrogen NuPAGE Novex), calibrated using SeeBlue Plus2 markers (Invitrogen). Quantification of protein bands by densitometry was performed with a GS-800 calibrated densitometer (Bio-Rad, Veenendaal, The Netherlands) relative to a calibration curve of the corresponding

protein isolated from the fermentation broth. (See the Results for purity.) The standard solution used to make the calibration curve was prepared by weighing a known amount of the isolated lyophilized protein. Blotting of proteins for N-terminal sequencing by Edman degradation was as previously described.[17] Protein sequencing was performed by Midwest Analytical (St. Louis, MO).

Rheometry. Data were acquired at 20 °C using a rheometer (Physica MCR 300) with Couette CC17 geometry and a bob and gap size of 8.5 and 0.7 mm, respectively. Of a stock solution containing 10 $g \cdot L^{-1}$ **CSSC** in 10 mM NaOH, 4.8 mL was quickly and thoroughly mixed with 948 μL of 250 mM HCl and 252 μL of water to reach a pH of approximately 1.5. Immediately after mixing, 4.2 mL was loaded in the thermostatted rheometer, and the pH in the remaining liquid was verified. A layer of oil was used to minimize evaporation. While the gel developed, the storage and loss moduli were monitored during 20 h at a strain of 0.1% and an oscillation frequency of 1 Hz so as to confirm that the moduli were stable before the strain was increased. Subsequently, the strain was increased stepwise, as indicated in Figure 2, and the stress was measured during 1 min at each strain level.

Microscopy. A stock solution (1 $g \cdot L^{-1}$) of **CSSC** or **SCCS** in 1 mM NaOH was diluted with 10 mM HCl to a final product concentration of 0.1 $g \cdot L^{-1}$ and left overnight at room temperature to allow supramolecular assembly. The resulting dispersion was used to prepare samples for AFM as well as TEM and cryo-TEM.

For imaging of supramolecular structures by AFM, a piece of clean hydrophilic silica wafer was dipped in the **CSSC** or **SCCS** dispersion, rinsed with dematerialized water, dried under a stream of nitrogen, and analyzed using a Digital Instruments NanoScope III in tapping mode with a Nano World SSS-NCH AFM probe having a typical radius of curvature of 2 nm, with a guaranteed maximum of 5 nm.

For imaging by TEM, a grid covered with Formvar film was first contacted with a drop of the **CSSC** or **SCCS** dispersion and then with a drop of 20 $g \cdot L^{-1}$ uranyl acetate (as a staining agent) in water (pH 3.7). It was subsequently air dried and viewed using a JEOL JEM 1200 EX II microscope operated at 80 kV. Digital images were recorded with KeenView/iTEM (SIS, Munster, Germany).

For cryo-TEM, an aliquot of 3 μL of sample solution was pipetted onto a glow-discharged Quantifoil R2/2 copper grid 200 mesh in the environmental chamber of a Vitrobot at a relative humidity of 100%. The sample was blotted once during 0.5 s and was rapidly plunged into liquid ethane. The grid was subsequently transferred to a Gatan cryoholder Model 626 and viewed in a Philips Tecnai12 TEM equipped with a Biotwin-lens and a LaB6 filament. Images were recorded with a SIS Megaview II CCD-camera and processed with AnalySIS software.

Small-Angle X-ray Scattering. We prepared a gel of CSSC or SCCS by dissolving 0.1 g freeze-dried material in 1 mL of 100 mM NaOH and 3.74 mL of water and then adding 0.26 mL of 1 M HCl to lower the pH and cause gelling. The samples were allowed to gel for several days in glass vials before core samples were taken by pushing 2 mm Kapton capillaries into the gels. SAXS measurements were performed on the samples contained in the capillaries at the ESRF in Grenoble (France) on the BM26B Dutch-Belgian beamline (DUBBLE) with an X-ray photon energy of 13 keV and a sample-to-detector distance of 4040 mm.[43] The acquisition time per image was 200 s, and the explored d range was 52.2−2.5 nm. Information about the shape and dimensions of the scattering objects was obtained via Guinier analysis

Circular Dichroism Spectroscopy. CD spectra were recorded between 190 and 260 nm on a Jasco J-715 spectropolarimeter at 21 °C with a resolution of 0.2 nm and a scanning speed of 1 $nm \cdot s^{-1}$. The spectra shown are the average of 15 recorded spectra. We prepared samples of **CSSC** or **SCCS** at different pH values by mixing a 1 $g \cdot L^{-1}$ **CSSC** or **SCCS** stock solution in 1 mM NaOH with water and 1 M HCl, resulting in final polymer concentrations of 0.1 $g \cdot L^{-1}$ at pH 7 and 0.09 $g \cdot L^{-1}$ at pH 2. A small sample was transferred to a 1 mm quartz cuvette for CD measurements, after which the pH of the remaining fluid was verified.

Acknowledgment. We thank Antoine Moers (A&F, Wageningen UR) for help with fermentations and protein purification, Adrie Westphal, Adriaan van Aelst and Luben Arnaudov (all of Wageningen University) for help with CD measurements, electron microscopy, and atomic force microscopy, respectively, and Hans Meeldijk (Electron Microscopy Department, Utrecht University) for perfoming cryo-TEM. This work is part of the Research Programme of the Dutch Polymer Institute (DPI), Eindhoven, The Netherlands, project no. 414.

Supporting Information Available: Cross sections of **CSSC** and **SCCS** fibrils were measured in AFM micrographs. The raw cryo-TEM image used to produce Figure 4 is given. SAXS data is presented, together with the model used to determine the size of the **S**-block tape core. This material is available free of charge via the Internet at http://pubs.acs.org.

References and Notes

(1) Park, M.; Harrison, C.; Chaikin, P. M.; Register, R. A.; Adamson, D. H. *Science* **1997**, *276*, 1401–1404.
(2) Muthukumar, M.; Ober, C. K.; Thomas, E. L. *Science* **1997**, *277*, 1225–1232.
(3) Krausch, G.; Magerle, R. *Adv. Mater.* **2002**, *14*, 1579–1583.
(4) Chen, C. S.; Mrksich, M.; Huang, S.; Whitesides, G. M.; Ingber, D. E. *Science* **1997**, *276*, 1425–1428.
(5) Silva, G. A.; Czeisler, C.; Niece, K. L.; Beniash, E.; Harrington, D. A.; Kessler, J. A.; Stupp, S. I. *Science* **2004**, *303*, 1352–1355.
(6) Harrington, D. A.; Cheng, E. Y.; Guler, M. O.; Lee, L. K.; Donovan, J. L.; Claussen, R. C.; Stupp, S. I. *J. Biomed. Mater. Res., Part A* **2006**, *78A*, 157–167.
(7) Chitkara, D.; Shikanov, A.; Kumar, N.; Domb, A. J. *Macromol. Biosci.* **2006**, *6*, 977–990.
(8) Woolfson, D. N.; Ryadnov, M. G. *Curr. Opin. Chem. Biol.* **2006**, *10*, 559–567.
(9) Mori, H.; Muller, A. H. E. *Prog. Polym. Sci.* **2003**, *28*, 1403–1439.
(10) Winnik, M. A.; Yekta, A. *Curr. Opin. Colloid Interface Sci.* **1997**, *2*, 424–436.
(11) Krejchi, M. T.; Atkins, E. D. T.; Waddon, A. J.; Fournier, M. J.; Mason, T. L.; Tirrell, D. A. *Science* **1994**, *265*, 1427–1432.
(12) Parkhe, A. D.; Cooper, S. J.; Atkins, E. D. T.; Fournier, M. J.; Mason, T. L.; Tirrell, D. A. *Int. J. Biol. Macromol.* **1998**, *23*, 251–258.
(13) Werten, M. W. T.; Moers, A. P. H. A.; Vong, T. H.; Zuilhof, H.; van Hest, J. C. M.; de Wolf, F. A. *Biomacromolecules* **2008**, *9*, 1705–1711.
(14) Werten, M. W. T.; Wisselink, W. H.; Jansen-van den Bosch, T. J.; de Bruin, E. C.; de Wolf, F. A. *Protein Eng.* **2001**, *14*, 447–454.
(15) Rozkiewicz, D. I.; Kraan, Y.; Werten, M. W. T.; de Wolf, F. A.; Subramaniam, V.; Ravoo, B. J.; Reinhoudt, D. N. *Chem.—Eur. J.* **2006**, *12*, 6290–6297.
(16) Bouwstra, J. B.; Toda, Y. *Recombinant Gelatin-Like Proteins for Use As Plasma Expanders*. U.S. Patent 7459431, June 2, **2005**.
(17) Werten, M. W. T.; Van den Bosch, T. J.; Wind, R. D.; Mooibroek, H.; De Wolf, F. A. *Yeast* **1999**, *15*, 1087–1096.
(18) Cereghino, G. P. L.; Cereghino, J. L.; Ilgen, C.; Cregg, J. M. *Curr. Opin. Biotechnol.* **2002**, *13*, 329–332.
(19) Smeenk, J. M.; Otten, M. B. J.; Thies, J.; Tirrell, D. A.; Stunnenberg, H. G.; van Hest, J. C. M. *Angew. Chem., Int. Ed.* **2005**, *44*, 1968–1971.
(20) Topilina, N. I.; Higashiya, S.; Rana, N.; Ermolenkov, V. V.; Kossow, C.; Carlsen, A.; Ngo, S. C.; Wells, C. C.; Eisenbraun, E. T.; Dunn, K. A.; Lednev, I. K.; Geer, R. E.; Kaloyeros, A. E.; Welch, J. T. *Biomacromolecules* **2006**, *7*, 1104–1111.
(21) Crisma, M.; Fasman, G. D.; Balaram, H.; Balaram, P. *Int. J. Pept. Protein Res.* **1984**, *23*, 411–419.
(22) Lednev, I. K.; Ermolenkov, V. V.; Higashiya, S.; Popova, L. A.; Topilina, N. I.; Welch, J. T. *Biophys. J.* **2006**, *91*, 3805–3818.
(23) Xu, B.; Yekta, A.; Li, L.; Masoumi, Z.; Winnik, M. A. *Colloids Surf., A* **1996**, *112*, 239–250.
(24) Krejchi, M. T.; Cooper, S. J.; Deguchi, Y.; Atkins, E. D. T.; Fournier, M. J.; Mason, T. L.; Tirrell, D. A. *Macromolecules* **1997**, *30*, 5012–5024.
(25) Chen, C. C.; Krejchi, M. T.; Tirrell, D. A.; Hsu, S. L. *Macromolecules* **1995**, *28*, 1464–1469.
(26) Greenfield, N.; Fasman, G. D. *Biochemistry* **1969**, *8*, 4108–4116.
(27) Iizuka, E.; Yang, J. T. *Biochemistry* **1968**, *7*, 2218–2228.
(28) Dicko, C.; Knight, D.; Kenney, J. M.; Vollrath, F. *Int. J. Biol. Macromol.* **2005**, *36*, 215–224.
(29) Lotz, B.; Keith, H. D. *J. Mol. Biol.* **1971**, *61*, 201–202.

(30) Asakura, T.; Ohgo, K.; Komatsu, K.; Kanenari, M.; Okuyama, K. *Macromolecules* **2005**, *38*, 7397–7403.
(31) Anderson, J. P.; Cappello, J.; Martin, D. C. *Biopolymers* **1994**, *34*, 1049–1058.
(32) Cui, X. Y.; Lee, V. A.; Raphael, Y.; Wiler, J. A.; Hetke, J. F.; Anderson, D. J.; Martin, D. C. *J. Biomed. Mater. Res.* **2001**, *56*, 261–272.
(33) Moselhi, A. *Br. J. Clin. Pract.* **1965**, *19*, 137–139.
(34) Gabrielli, F.; Potenza, C.; Puddu, P.; Sera, F.; Masini, C.; Abeni, D. *Plast. Reconstr. Surg.* **2001**, *107*, 38–45.
(35) Boyd, L. M.; Carter, A. J. *Eur. Spine J.* **2006**, *15*, S414–S421.
(36) Ramshaw, J. A.; Werkmeister, J. A.; Glattauer, V. *Biotechnol. Genet. Eng. Rev.* **1996**, *13*, 335–382.
(37) Pachence, J. M. *J. Biomed. Mater. Res.* **1996**, *33*, 35–40.
(38) Lee, C. H.; Singla, A.; Lee, Y. *Int. J. Pharm.* **2001**, *221*, 1–22.
(39) Brown, R. A.; Phillips, J. B. *Int. Rev. Cytol.* **2007**, *262*, 75–150.
(40) Liu, C. Y.; Apuzzo, M. L.; Tirrell, D. A. *Neurosurgery* **2003**, *52*, 1154–1165, and discussion 1165−1157.
(41) Werten, M. W. T.; de Wolf, F. A. *Appl. Environ. Microbiol.* **2005**, *71*, 2310–2317.
(42) Dubois, M.; Gilles, K. A.; Hamilton, J. K.; Rebers, P. A.; Smith, F. *Anal. Chem.* **1956**, *28*, 350–356.
(43) Borsboom, M.; Bras, W.; Cerjak, I.; Detollenaere, D.; Glastra Van Loon, D.; Goedtkindt, P.; Konijnenburg, M.; Lassing, P.; Levine, Y. K.; Munneke, B.; Oversluizen, M.; Van Tol, R.; Vlieg, E. *J. Synchrotron Radiat.* **1998**, *5*, 518–520.

MA801955Q